The Association Between Imaging Features of TSCT and the Expression of PD-L1 in Patients With Surgical Resection of Lung Adenocarcinoma

Tong Wu,[1] Fei Zhou,[2] Adiilah K. Soodeen-Lalloo,[1] Xing Yang,[1] Yingran Shen,[3] Xi Ding,[4] Jinpeng Shi,[2] Jie Dai,[3] Jingyun Shi[1]

Abstract

In this study we identified 350 patients with pathologically confirmed adenocarcinoma. Of 350 specimens, 74 (21.1%) were programmed death-ligand 1-positive. In multivariate analysis, absence of surrounding ground glass opacity ($P = .022$), shape ($P = .008$), pleural indentation ($P = .007$), tumor mean computed tomography value ($P = .004$), and the ratio of consolidation mass to tumor mass ($P = .003$) were significantly associated with programmed death-ligand 1 expression.

Objectives: Programmed death-ligand 1 (PD-L1) expression might serve as a predictive biomarker for immune checkpoint inhibitors in lung cancer. However, the relationship between PD-L1 expression and imaging features of lung cancer has not been fully understood. **Patients and Methods:** A total of 350 patients with pathologically confirmed adenocarcinoma who received surgical treatment and had preoperative thin section computed tomography (CT) examination were included. Quantitative CT features including the mean CT value and tumor mass were measured on multiplanar reconstructed images. PD−L1-positive tumor was defined as the tumor proportion score $> 5\%$. **Results:** Seventy-four of 350 (21.1%) specimens were detected as PD−L1-positive tumors. PD-L1 expression was adversely associated with epidermal growth factor receptor mutation status ($P < .001$) and was significantly associated with invasive adenocarcinomas rather than preinvasive lesions and minimally invasive adenocarcinomas ($P < .001$). Multivariate analysis identified absence of surrounding ground glass opacity ($P = .022$), shape ($P = .008$), pleural indentation ($P = .007$), tumor mean CT value ($P = .004$), and the ratio of consolidation mass to tumor mass ($P = .003$) as being significantly associated with the expression of PD-L1. To improve the diagnostic accuracy, a joint model that combined 5 imaging traits was conducted. The area under the curve of the joint model was 0.783, with a sensitivity of 81.1% and specificity of 64.1%, respectively. **Conclusion:** PD-L1 expression was associated with pathologic invasiveness of adenocarcinomas and CT features, which suggested the possibility of predicting PD-L1 expression status via imaging features.

Clinical Lung Cancer, Vol. 20, No. 2, e195-207
Keywords: CT, Epidermal growth factor receptor, Immunotherapy, Invasive, Programmed death-ligand 1

Introduction

Lung cancer is the major cause of cancer-related mortality worldwide and non−small-cell lung cancer (NSCLC) accounts for approximately 85% of all cases. Lung adenocarcinoma is the most common pathological subtype of NSCLC.[1] Because of a lack of obvious early symptoms, most patients are diagnosed at advanced stages and miss the best time for treatment.[2] Chemotherapy is still the standard treatment for patients with advanced NSCLC but has many side effects and the overall prognosis is still poor.[3] Recently, molecular targeted therapy has profoundly changed the survival

T.W. and F.Z. contributed equally to this work.

[1]Department of Radiology, Shanghai Pulmonary Hospital, Tongji University School of Medicine, Shanghai, China
[2]Department of Medical Oncology, Shanghai Pulmonary Hospital and Thoracic Cancer Institute, Tongji University School of Medicine, Shanghai, China
[3]Department of Thoracic Surgery, Shanghai Pulmonary Hospital, Tongji University, Shanghai, China
[4]Central Laboratory, Shanghai Pulmonary Hospital, Tongji University School of Medicine, Shanghai, China

Submitted: May 14, 2018; Revised: Oct 31, 2018; Accepted: Oct 31, 2018; Epub: Nov 14, 2018

Addresses for correspondence: Jingyun Shi, MD, Department of Radiology, Shanghai Pulmonary Hospital, Tongji University, 507 Zhengmin Rd, Shanghai 200433, P.R. China and Jie Dai, MD, PhD, Department of Thoracic Surgery, Shanghai Pulmonary Hospital, Tongji University, 507 Zhengmin Rd, Shanghai 200433, P.R. China
E-mail contact: drshijingyun@126.com; tjdj1021@163.com

1525-7304/$ - see frontmatter
https://doi.org/10.1016/j.cllc.2018.10.012

outcomes of patients with actionable molecular abnormalities, including epidermal growth factor receptor (*EGFR*) sensitizing mutations, anaplastic lymphoma kinase (*ALK*) translocations, and C-ros oncogene 1 receptor tyrosine kinase (*ROS1*) translocations.[4,5] Previous studies have shown that compared with conventional chemotherapy, targeted therapies manifest modest toxicities but better clinical efficacy, with improved objective response rate and progression-free survival.[6-8] However, acquired resistance inevitably develops after 10 to 14 months.[9] The emergence of drug resistance leads to the bottleneck of molecular targeted therapy. Therefore, novel treatment paradigms are urgently needed to further improve the prognosis of NSCLC patients.

In recent years, monoclonal antibody against immune checkpoints has made breakthroughs across many tumor types, especially in melanoma, lung cancer, kidney cancer, and bladder cancer.[10] A series of clinical trials have confirmed the efficacy and safety of programmed death 1 (PD-1)/programmed death-ligand 1 (PD-L1) inhibitors in second-line treatment of NSCLC.[11] The activation of the PD-1/PD-L1 pathway can help tumor cells escape T-cell cytolysis and facilitate cancer formation. Immune checkpoint inhibitors (ICIs) can reactivate T-cell activity by directly binding PD-1 or its ligand PD-L1, blocking the PD-1/PD-L1 pathway, and hence eliminate tumor cells. Multiple studies have shown that PD-L1 expression on tumor cells might predict the response to ICIs, including in lung cancer.[11,12] Therefore, it is very important to evaluate the status of PD-L1 expression to help identify patients who might benefit from ICI therapy.[13]

Currently, the detection of PD-L1 expression is mainly on the basis of biopsy or resection specimens.[14] However, sometimes there is no sufficient tumor sample for PD-L1 staining, so it is not suitable for all patients, especially for patients with advanced diseases. Therefore, less invasive approaches are needed to help predict PD-L1 expression.[15] It has previously been reported that imaging features of computed tomography (CT) were associated with the status of genetic alterations, such as *EGFR*, Kirsten rat sarcoma viral oncogene (*KRAS*), *ALK* alternations.[16,17] Hence, if the expression of PD-L1 can be determined according to specific CT imaging features, it might be helpful for patients who are expected to receive ICIs and do not have enough tumor tissue for the evaluation of PD-L1 expression.

Therefore, the purpose of the current study was to identify particular imaging findings that might be associated with PD-L1 expression in patients with surgical resection of lung adenocarcinoma.

Patients and Methods

Patient Selection

We retrospectively examined patients who were diagnosed pathologically with adenocarcinomas and underwent radical surgical resection of solitary pulmonary nodule in Shanghai Pulmonary Hospital from May 2017 to September 2017. During this period, 396 patients were identified. Among them, 10 had no preoperative thin section CT (TSCT) data on picture archiving and communication systems, and 30 had no *EGFR* mutational status data and were excluded from the study. Finally, 350 patients with adenocarcinomas were included for further analysis. The study was approved by the ethic committee of Shanghai Pulmonary Hospital and informed consent was obtained from every participant before the initiation of any study-related procedure.

Image Acquisition

According to previous image acquisition methods,[18] all patients were instructed to hold their breath in full-inhalation for the whole scan period. CT scans ranged from thoracic inlet to subcostal plane and were obtained before surgical resection from 2 CT machines: Brilliance (Philips Medical Systems Inc, Cleveland, OH) and SOMATOM Definition AS (Siemens Aktiengesell-schaft, Munich, Germany). CT parameters of Brilliance (Philips Medical Systems Inc) were as follows: 64 × 1 mm acquisition; 0.75-second rotation time; slice width 1 mm; tube voltage, 120 kVp; tube current, 150 to 200 mA; lung window center: −700 Hounsfield units (HU), and window width:1200 HU; mediastinal window center: 60 HU and window width: 450 HU level; pitch: 0.906; and field of view (FOV): 350 mm. CT parameters of the SOMATOM Definition AS (Siemens Aktiengesell-schaft) were as follows: 128 × 1 mm acquisition; 0.5-second rotation time; slice width: 1 mm; tube voltage: 120 kVp; tube current: 150 to 200 mA; lung window center: −700 HU and window width 1200 HU; and mediastinal window center: 60 HU and window width: 450 HU level; FOV: 300 mm; pitch: 1.2; and FOV: 350 mm. TSCT images were reconstructed into 0.67- to 1.25-mm section thicknesses according to a high-resolution algorithm. TSCT images were analyzed with pulmonary nodules assessment software (IntelliSpace Portal, Radiology DICOM image processing application software, 459801225931, Philips Medical Systems Inc), in which 3-dimensional nodules can be reconstructed by depicting a region of interest covering as large an area as possible from the whole tumor on axial plane. Meanwhile, coronal and sagittal images corresponding to each cross-section of the nodule helped the radiologist determine whether the outlined contour was accurate (Figure 1). If it was inaccurate, it would be manually adjusted with an electronic cursor and mouse. At the end of the 3-dimensional segmentation, the following parameters were calculated according to this software automatically: maximal diameter, effective diameter, volume, and mean CT value (voxel-based noncontrast CT numbers were collected from the lesion segmentation).

Evaluation of TSCT Features

All categorical variables of TSCT images were reviewed by 2 experienced chest radiologists who were blinded to the history and pathological diagnosis of each patient. If there were significant differences between the radiologists, a decision would be reached in consensus. The following categorical variables were evaluated on TSCT: (1) surrounding ground glass opacity (GGO); (2) shape: round, lobular, or irregular shape; (3) margin: smooth, speculated, or lobulated; (4) adenocarcinoma with cyst or without; (5) air bronchogram; (6) vessel convergence sign; (7) vascular invasion; and (8) pleural indentation. The kappa indices for the categorical variables mentioned previously were > 0.800.

The quantitative variables included the following: (1) size (in millimeters), volume (unit: in cubic millimeters), and mean CT value (HU) of the consolidation part and the whole tumor, respectively, and maximum diameter of the whole tumor (millimeters) on the basis of the 3-dimensional reconstruction; (2) mass, calculated as volume × (mean CT value + 1000)/1000[19]; (3) the

Figure 1 At Each Cross-Sectional Level of the Lesion, a Coronal Image and a Sagittal Image Are Shown at the Same Time to Help the Radiologist Accurately Trace the Entire Nodule (A-F). Three-Dimensional Reconstruction Can Clearly Show the Surrounding Condition of the Nodule and Pleural Indentation (G and H)

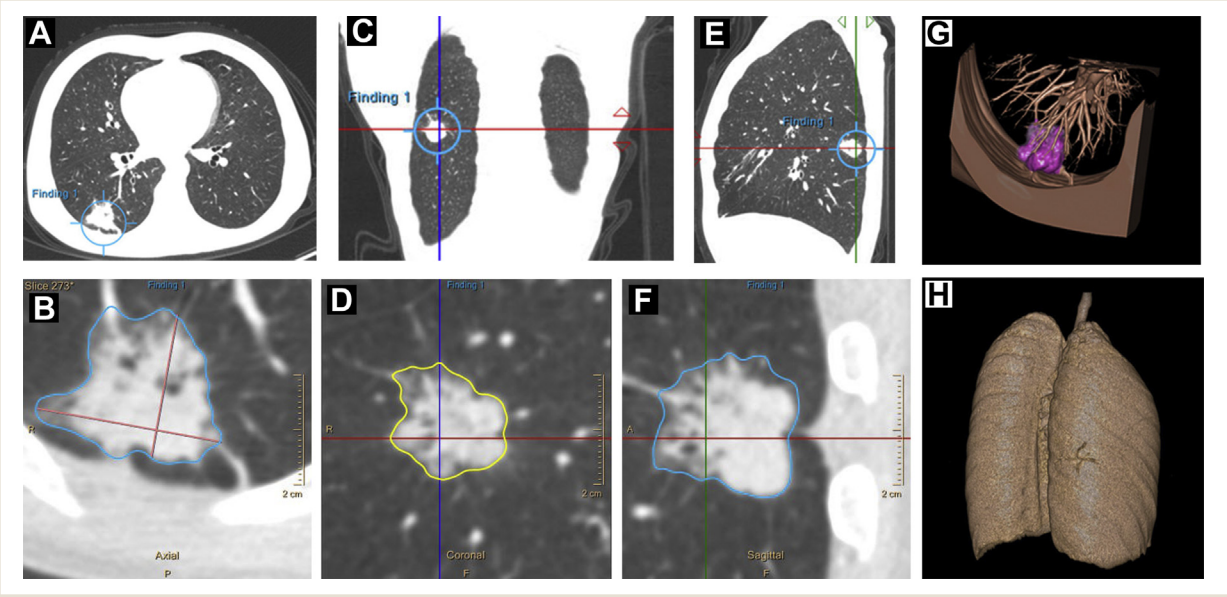

consolidation part to the whole tumor ratio of size (C/T size), volume (C/T volume), and mass (C/T mass). The measurements were performed by 1 radiologist, which lasted for 1 month to finish the first round of evaluation. After the first evaluation was finished, the radiologist repeated the second evaluation again nearly 1 month later. If the difference of the measured variables was more than 10% compared with the first measurement, the variables would be re-evaluated by a second radiologist. Any disagreements would be resolved in consensus. The intraclass correlation coefficient values ranged from 0.813 to 0.956 for CT quantitative indicators.

Pathologic Diagnosis

All surgical specimens were fixed in 10% formalin, embedded in paraffin, sectioned with a microtome, and stained with hematoxylin and eosin. Pathologic analysis was done by 2 experienced pathologists in consensus using the criteria of 2011 international Association for the Study of Lung Cancer/American Thoracic Society/European Respiratory Society multidisciplinary classification of lung adenocarcinoma.[20]

Immunohistochemical Analysis

The paraffin section was cut to a thickness of 4 μm on a microtome and placed on a slide coated with polylysine, and the wafer was ready for dewaxing in xylene, hydrated in graded alcohols, washed with phosphate-buffered saline (PBS) for 5 minutes. After blocking endogenous peroxidase activity with 3% H_2O_2 aqueous solution for 10 minutes, the sections were incubated with primary antibodies at 4°C overnight. After washing with PBS, they were then incubated with secondary antibody at 37°C for 30 minutes. Finally, the sections were reacted in 3,3′-diaminobenzidine, restained with hematoxylin and then dehydrated in graded alcohols, cleared in xylene, and covered with coverslips. In this study, anti-human PD-L1 (13684, clone E1L3N; Cell Signaling Technology [Danvers, MA], diluted 1:200) was used as primary antibodies, and a peroxidase-labeled secondary antibody (REAL EnVision Detection Reagent Peroxidase Rabbit/Mouse; DAKO [Glostrup, Denmark]) was used to visualize the antigen. We set the cutoff values at 5% on the basis of previous clinical trials.[11] More than 5% of staining of the tumor cell membrane was defined as positive in a section that included at least 100 tumor cells that could be evaluated. All immunohistochemical (IHC) analyses were evaluated by 2 experienced pathologists who were blinded to identity of the specimens and gave consistent results of the consultation with a kappa index of 0.968.

Statistical Analysis

The relationship between PD-L1 expression and clinicopathological characteristics was analyzed using χ^2 test or the Fisher exact text (as appropriate) for categorical variables and using independent samples Mann−Whitney *U* test for continuous variables. All imaging features were put in univariate and multivariate logistic regression analyses. The receiver operating characteristic (ROC) curves were generated to determine the threshold of significant indicators and to evaluate differentiating performance of the logistic regression model. The cutoff value was determined when the Youden index was maximal.

To identify the best diagnostic efficiency, area under the curve (AUC) was calculated for the significant parameters in multivariate logistic regression analysis. We compared the specificity and sensitivity of joint diagnostic model (including all significant imaging features in multivariate logistic regression analysis) with radiological measurement index only (tumor mean CT value or C/T mass) using

binary logistic regression analysis to determine whether a joint model could improve the diagnostic accuracy. Any P value $< .05$ was considered statistically significant on the basis of 2-sided testing. All statistical analyses were performed using SPSS version 19 (IBM Corp, Armonk, NY).

Results

Clinicopathological Characteristics

This study included 143 (40.9%) men and 207 (59.1%) women. Forty-two percent of patients were former or present smokers. The correlations between PD-L1 expression and clinicopathological characteristics are shown in Table 1. In brief, PD−L1-positive tumors were more commonly found in male patients ($P = .039$), former/present smokers ($P < .001$), invasive pathological subtype ($P < .001$), larger pathological tumor diameter ($P = .008$), higher Tumor, Node, Metastases (TNM) stage ($P = .001$), and *EGFR* wild type status ($P < .001$). In contrast, *EGFR* mutations were more frequently present in women, never smokers, and negative PD-L1 expression ($P < .001$), which are shown in Supplemental Table 1 in the online version.

Regarding pathological subtype, 95 patients were diagnosed with atypical adenomatous hyperplasia (AAH)/adenocarcinoma in situ (AIS)/minimally invasive adenocarcinoma (MIA), and 255 with invasive adenocarcinoma. The distribution of pathological subtype for PD-L1 expression is shown in Table 2 and Supplemental Figure 1 in the online version. PD−L1-positive tumors were more commonly identified in micropapillary predominant adenocarcinoma and solid predominant adenocarcinoma ($P < .001$).

Thin Section CT Features and Pathological Invasiveness

As shown in Table 3, invasive adenocarcinomas (including lepidic predominant adenocarcinoma, acinar predominant adenocarcinoma, papillary predominant adenocarcinoma, micropapillary predominant adenocarcinoma, and solid predominant adenocarcinoma) were more frequently present in patients with absence of surrounding GGO ($P < .001$), lobular/irregular shape ($P < .001$), speculated/lobulated margin ($P < .001$), adenocarcinomas with cysts ($P = .001$), air bronchogram ($P < .001$), vessel convergence sign ($P < .001$), vascular invasion ($P < .001$), and pleural indentation ($P < .001$) compared with the preinvasive lesions (AAH or AIS) and MIA.

Programmed Death-Ligand 1 Expression and Imaging Features

The results of the univariate and multivariate logistic regression analysis of PD-L1 expression status and TSCT features are shown in

Table 1 Programmed Death Ligand-1 Expression and Clinicopathological Characteristics

	PD−L1-Negative (n = 276)	PD−L1-Positive (n = 74)	Total	*P*
Sex, n (%)				
Male	105 (38.0)	38 (51.4)	143 (40.9)	.039
Female	171 (62.0)	36 (48.6)	207 (59.1)	
Mean Age, y	62.11 ± 9.48	62.12 ± 8.13	62.11 ± 9.20	.890
Smoking History, n (%)				
Ever smoker	94 (34.1)	53 (71.6)	147 (42.0)	.000
Never smoker	182 (65.9)	21 (28.4)	203 (58.0)	
Location, n (%)				
LUL	54 (19.6)	19 (25.7)	73 (20.9)	.509
LLL	39 (14.1)	9 (12.2)	48 (13.7)	
RUL	92 (33.3)	26 (35.1)	118 (33.7)	
RML	26 (9.4)	3 (4.1)	29 (8.3)	
RLL	65 (23.6)	17 (23.0)	82 (23.4)	
Pathological Diagnosis, n (%)				
AAH/AIS/MIA	90 (32.6)	5 (6.8)	95 (27.1)	.000
Invasive subtype	186 (67.4)	69 (93.2)	255 (72.9)	
Pathological Tumor Diameter, n (%), cm				
≤2.0	141 (51.1)	25 (33.8)	166 (47.4)	.008
>2.0	135 (48.9)	49 (66.2)	184 (52.6)	
TNM				
a	246 (89.1)	55 (74.3)	301 (86.0)	.001
≥Ib	30 (10.9)	19 (25.7)	49 (14.0)	
***EGFR* Mutation Status, n (%)**				
Wild type	95 (34.4)	50 (67.6)	145 (41.4)	.000
Mutant	181 (65.5)	24 (32.4)	205 (58.6)	

Abbreviations: AAH = atypical adenomatous hyperplasia; AIS = adenocarcinoma in situ; LLL = left lower lobe; LUL = left upper lobe; MIA = minimally invasive adenocarcinoma; PD-L1 = programmed death ligand-1; RLL = right lower lobe; RML = right middle lobe; RUL = right upper lobe; TNM = tumor, node, metastases.

Table 2 The Distribution of PD-L1 Expression in Different Subtypes

	PDPD−L1-Negative (n = 276)	PDPD−L1-Positive (n = 74)	Total	*P*
Pathological Diagnosis[a]				
AAH	13 (4.7)	0 (0.0)	13 (3.7)	.000
AIS	34 (12.3)	2 (2.7)	36 (10.3)	
MIA	43 (15.6)	3 (4.1)	46 (13.1)	
Lepidic predominant AD	51 (18.5)	11 (14.9)	62 (17.7)	
Acinar predominant AD	53 (19.2)	36 (48.6)	89 (25.4)	
Papillary predominant AD	70 (25.4)	7 (9.5)	77 (22.0)	
Micropapillary predominant AD	4 (1.4)	2 (2.7)	6 (1.7)	
Solid predominant AD	8 (2.9)	13 (17.6)	21 (6.0)	
Pathological Diagnosis[a]				
Other subtype	264 (95.7)	59 (79.7)	324 (92.3)	.000
Micropapillary predominant AD/solid predominant AD	12 (4.3)	15 (20.3)	27 (7.7)	

Data are presented as n (%) except where otherwise noted.
Abbreviations: AAH = atypical adenomatous hyperplasia; AD = adenocarcinoma; AIS = adenocarcinoma in situ; MIA = minimally invasive adenocarcinoma; PD-L1 = programmed death ligand-1.
[a]Two groups according to the poorer prognosis in clinic.

Table 4. In univariate logistic regression analysis, PD-L1 expression was significantly related to absence of surrounding GGO ($P < .001$), lobular/irregular shape ($P = .002$), speculated/lobulated margin ($P < .001$), vessel convergence sign ($P = .010$), vascular invasion ($P = .011$), larger size ($P < .001$), mean CT value ($P < .001$), volume ($P < .001$), and mass ($P < .001$) of the whole tumor and the consolidation part respectively, and higher C/T size ($P < .001$), C/T volume ($P < .001$), and C/T mass ($P < .001$). Multivariate logistic regression analysis showed the absence of surrounding GGO (odds ratio [OR], 0.4; 95% confidence interval [CI], 0.2-0.9; $P = .022$), lobular/irregular shape (OR, 5.8; 95% CI, 1.6-21.0; $P = .008$), pleural indentation (OR, 2.8; 95% CI, 1.3-5.7; $P = .007$), tumor mean CT value (OR, 4.9; 95% CI, 1.7-14.4; $P = .004$), and C/T mass (OR, 4.7; 95% CI, 1.7-13.0; $P = .003$) were significantly associated with PD-L1 expression. The ROC analysis determined the optimal cutoff values for tumor mean CT value at −170 HU and C/T mass at 30.9%. The AUC of the logistic regression analysis was 0.733 (sensitivity: 71.6%, specificity: 70.3%), and 0.705 (sensitivity: 82.4%, specificity: 60.1%). respectively (Figure 2). To improve the diagnostic accuracy, a joint diagnostic model was conducted as shown in Figure 2. The purpose of the joint diagnostic model is to simultaneously combine all significant imaging parameters that are significant in multivariate logistic regression analysis and analyze the diagnostic accuracy of multiple indicators for the identification of PD-L1 expression. The AUC of the joint diagnostic model was 0.783 (sensitivity: 81.1%, specificity: 64.1%). The results of the univariate logistic regression analysis of *EGFR* mutation and TSCT features are shown in Supplemental Table 2 in the online version. *EGFR* status was correlated to presence of surrounding GGO ($P = .022$), larger tumor maximum diameter ($P = .008$) and smaller C/T size ($P = .010$), C/T volume ($P = .010$), and C/T mass ($P = .010$).

Discussion

Immune checkpoint blockade, which targets regulatory pathways in T cells to improve antitumor immune responses, has led to important clinical advances and provided a new weapon against cancer.[14] The PD-1/PD-L1 pathway plays an important role in many aspects of the immune response. The promotion of tumor immune escape by this pathway mainly depends on the direct binding of PD-L1 expressed on tumor cells and PD-1 expressed on T lymphocytes. Therefore, the expression of PD-L1 on the surface of tumor cells might be an important predictive biomarker for anti−PD-1/PD-L1 immunotherapy.[13,14,21] If an association between PD-L1 expression and radiological phenotype could be established, it could be used to reflect the response to ICIs. However, to our knowledge, the correlation between PD-L1 expression and radiological features was not well studied.

In our study, the positive rate of PD-L1 expression was 21.1% and PD-L1 expression was more frequently present in men and former or present smokers. This result was similar to previous retrospective study showing that smoking status could induce PD-L1 expression.[22] On the contrary, *EGFR* mutations were more common in women and never smokers, which was also reported.[23] Our study showed that adenocarcinomas with PD-L1 expression had higher pathological tumor size, advanced TNM stage, and a higher proportion of invasive adenocarcinoma. Shimoji et al[24] reported that PD-L1 expression was closely associated with higher pathological grade and worse pathological subtype. Russell et al reported micropapillary predominant and solid predominant adenocarcinomas were associated with poor survival.[25] These findings indicated that patients with PD-L1 expression might have worse prognosis and related studies have documented that patients with PD-L1 expression could be predicted to present a poorer long-term survival.[15] It is worth mentioning that in our study, *EGFR* mutation was inversely associated with the expression of PD-L1. Azuma et al suggested that PD-L1 expression was positively associated with *EGFR* mutation.[26] This difference might because most of our patients were at an early stage of adenocarcinoma and we excluded other types of lung cancer.

Our results suggest that PD-L1 expression is related to the absence of surrounding GGO. In the process of tumorigenesis, the lepidic growth pattern of adenocarcinoma replacing the alveolar wall

Table 3 Pathological Invasiveness and Imaging Features

	AAH/AIS/MIA (n = 95)	IA (n = 255)	*P*
Surrounding GGO, n (%)			
No	1 (1.1)	115 (45.1)	.000
Yes	94 (98.9)	140 (54.9)	
Shape, n (%)			
Round	54 (56.8)	10 (3.9)	.000
Lobular/irregular	41 (43.2)	245 (96.1)	
Margin, n (%)			
Smooth	95 (100.0)	136 (53.3)	.000
Speculated/lobulated	0 (0.0)	119 (46.7)	
Cyst, n (%)			
No	93 (97.9)	218 (85.5)	.001
Yes	2 (2.1)	37 (14.5)	
Air Bronchogram, n (%)			
No	78 (82.1)	87 (34.1)	.000
Yes	17 (17.9)	168 (65.9)	
Vessel Convergence Sign, n (%)			
No	91 (95.8)	147 (57.6)	.000
Yes	4 (4.2)	108 (42.4)	
Vascular invasion, n (%)			
No	95 (100.0)	203 (79.6)	.000
Yes	0 (0.0)	52 (20.4)	
Pleural Indentation, n (%)			
No	72 (75.8)	55 (21.6)	.000
Yes	23 (24.2)	200 (78.4)	
Tumor Maximum Diameter, mm	11.13 ± 6.25	28.08 ± 8.34	.000
Tumor			
Size, mm	7.92 ± 3.76	19.03 ± 5.11	.000
Mean CT, HU	−469.38 ± 167.70	−265.56 ± 241.86	.000
Volume, mm^3	512.60 ± 1503.40	4386.43 ± 3418.76	.000
Mass	259.82 ± 826.23	3111.64 ± 2307.61	.000
Consolidation			
Size, mm	1.33 ± 2.75	12.73 ± 7.44	.000
Mean CT, HU	−429.29 ± 197.40	−129.60 ± 175.93	.000
Volume, mm^3	39.60 ± 136.34	2057.93 ± 2347.38	.000
Mass	35.26 ± 120.97	1999.29 ± 2362.96	.000
C/T			
Size, mm	0.15 ± 0.30	0.66 ± 0.37	.000
Volume, mm^3	0.09 ± 0.22	0.52 ± 0.45	.000
Mass	0.10 ± 0.24	0.55 ± 0.44	.000

Data are presented as n (%) or mean ± SD, except where otherwise noted.
Abbreviations: AH = atypical adenomatous hyperplasia; AIS = adenocarcinoma in situ; CT = computed tomography; C/T = the ratio of consolidation part to the whole tumor; GGO = ground glass opacity; HU = Hounsfield units; IA = invasive adenocarcinoma; MIA = minimally invasive adenocarcinoma.

presents as GGO on TSCT. In contrast, a solid component on TSCT indicated collapse of the alveolar wall, fibrosis, or proliferation of invasive tumor cells.[27] Dai et al[16] reported the association of a percentage of the solid component on TSCT with the extent of pathologic invasiveness. From a histomorphology point of view, solid and micropapillary dominant tumors have greater malignant potential than GGO-based tumors. It can be deduced that PD-L1 expression was significantly associated with a more aggressive pathological type of adenocarcinoma. However, we also showed that the presence of surrounding GGO was significantly associated with *EGFR* mutation. It was reported that under the premise of the Noguchi classification, a higher mutation rate was found in Noguchi A, B, and C (containing ground glass components) than Noguchi D, E, and F (solid lesions).[28] This could partially explain

Table 4 Programmed Death Ligand-1 Expression and Imaging Features

	PD-L1		Univariate Analysis		Multivariate Analysis	
	Negative (n = 276)	Positive (n = 74)	OR (95% CI)	*P*	OR (95% CI)	*P*
Surrounding GGO						
No	76 (27.5)	41 (55.4)	0.3 (0.2-0.5)	.000	0.4 (0.2-0.9)	.022
Yes	200 (72.5)	33 (44.6)				
Shape						
Round	61 (22.1)	3 (4.1)	6.7 (2.0-22.1)	.002	5.8 (1.6-21.0)	.008
Lobular/irregular	215 (77.9)	71 (95.9)				
Margin						
Smooth	202 (73.2)	29 (39.2)	4.2 (2.5-7.2)	.000		
Speculated/lobulated	74 (26.8)	45 (60.8)				
Cyst						
No	244 (88.4)	67 (90.5)	0.8 (0.3-1.9)	.605		
Yes	32 (11.6)	7 (9.5)				
Air Bronchogram						
No	133 (48.2)	32 (43.2)	1.2 (0.7-2.0)	.450		
Yes	143 (51.8)	42 (56.8)				
Vessel Convergence Sign						
No	197 (71.4)	41 (55.4)	2.0 (1.2-3.4)	.010		
Yes	79 (28.6)	33 (44.6)				
Vascular Invasion						
No	242 (87.7)	56 (75.7)	2.3 (1.2-4.3)	.011		
Yes	34 (12.4)	18 (24.3)				
Pleural Indentation						
No	105 (38.0)	22 (29.7)	1.5 (0.8-2.5)	.188	2.8 (1.3-5.7)	.007
Yes	171 (62.0)	52 (70.3)				
Tumor Maximum Diameter, mm	28.23 ± 14.31	30.25 ± 9.40	5.7 (2.2-14.7)	.000		
Tumor						
Size, mm	19.07 ± 9.29	21.27 ± 5.62	6.9 (2.4-19.5)	.000		
Mean CT, HU	−330.05 ± 228.85	−139.57 ± 197.69	6.0 (3.4-10.5)	.000	4.9 (1.7-14.4)	.004
Volume, mm^3	6226.86 ± 6956.52	6024.92 ± 4065.80	6.9 (2.4-19.5)	.000		
Mass	4305.35 ± 5029.65	5173.48 ± 3439.61	2.9 (1.7-5.1)	.000		
Consolidation						
Size, mm	10.85 ± 9.80	17.25 ± 7.90	4.9 (2.8-8.5)	.000		
Mean CT, HU	−214.12 ± 234.51	−66.92 ± 143.26	3.6 (2.1-6.2)	.000		
Volume, mm^3	2482.86 ± 4448.40	4118.02 ± 3208.20	5.2 (3.0-9.0)	.000		
Mass	2373.43 ± 4282.00	4051.19 ± 3204.32	4.9 (2.9-8.5)	.000		
C/T						
Size, mm	0.49 ± 0.40	0.80 ± 0.32	6.6 (3.5-12.3)	.000		
Volume, mm^3	0.36 ± 0.42	0.70 ± 0.39	6.6 (3.5-12.3)	.000		
Mass	0.38 ± 0.42	0.72 ± 0.37	7.1 (3.7-13.5)	.000	4.7 (1.7-13.0)	.003

Data are presented as n (%) or mean ± SD, except where otherwise noted.
Abbreviations: CT = computed tomography; GGO = ground glass opacity; HU = Hounsfield units; OR = odds ratio; C/T = the ratio of consolidation part to the whole tumor; PD-L1 = programmed death ligand-1.

why *EGFR* mutation is closely related to the lepidic predominant growth characteristic of adenocarcinoma, whereas the lepidic predominant adenocarcinoma is closely related to the GGO on CT.[28]

Our study showed that lobular/irregular shape and pleural indentation were associated with PD-L1 expression. Lobular/irregular shape and pleural indentation were both considered as significant imaging features distinguishing malignancy from benign pulmonary tumors. The occurrence of lobulated sign was related to the proliferation of tumor in the lobule, the growth velocity of various parts of the tumor, the incomplete septa, lymphatic spread, and airway spread.[29] Pleural indentation was considered to represent thickened fibrous strands along the interlobar septa between the

Figure 2 Receiver Operating Characteristic Analysis of Tumor Mean Computed Tomography (CT) Value, the Consolidation Part to the Whole Tumor Ratio of Mass (C/T Mass) and Joint Model. The Receiver Operating Characteristic Curve for Detecting Programmed Death-Ligand 1 (PD-L1) Expression. The Cutoff, Area Under the Curve, Sensitivity, Specificity at Cutoff of Tumor Mean CT Value, and C/T Mass Were: 170 Hounsfield Units and 30.9%; 0.733 and 0.705; 71.62% and 82.43%; 70.29% and 60.14%, Respectively, Between the PD−L1-Positive Group and Negative Group. The Area Under the Curve of the Joint Diagnostic Model Was 0.783 (95% CI, 0.724-0.843), Which Was Considered to Be Highly Accurate.

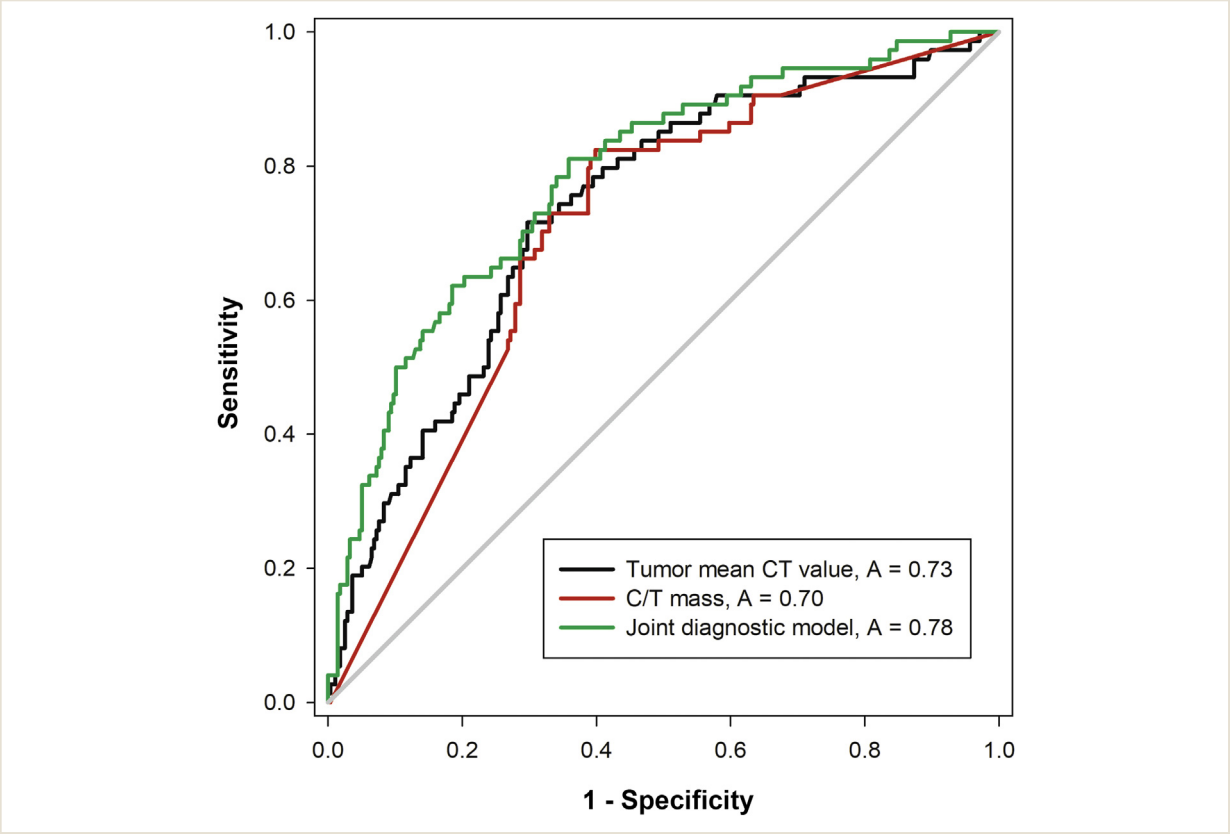

Abbreviation: A = area under the curve.

tumor and the pleural surface.[30] Both signs were typical imaging features of invasive adenocarcinoma. As discussed previously, PD-L1 expression is more likely to be found in worse pathologic subtypes. Besides, we found that there was no significant correlation between PD-L1 expression and cyst. Toyokawa et al concluded that adenocarcinomas with cyst were significantly associated with PD-L1 expression.[31] We have drawn different conclusions because of the different mechanisms of cyst formation in adenocarcinomas. The most common mechanism includes invasion of the alveolar wall and bronchial wall. This leads to wall thickening and narrowing of the small airways, or clogging of the valves, resulting in an increase in the volume and pressure of the intracavity gas and hence cyst is formed. Woodring et al reported the degree of differentiation among lung adenocarcinomas with cysts as well, suggesting that the prognosis was better.[32] It could help explain the adverse correlation between PD-L1 expression and cyst in our study.

Moreover, we found that tumor mean CT value and C/T mass were significantly correlated with PD-L1 expression. Tumor mean CT value reflected the attenuation of x-rays by the tumor and the density of the tumor tissue. For example, Lee et al indicated that if pure ground glass nodules had high pixel attenuation, the nodules were more likely to be invasive adenocarcinomas.[33] We validated that tumor mean CT value was an independent differentiating factor between the PD−L1-positive group and negative group with a cutoff value of −170 HU. If the mean CT value of a tumor is greater than −170 HU, it is more likely to contain solid components and the presentation is more likely to be a pathological subtype with poor prognosis. However, we found that higher C/T size, C/T volume, and C/T mass were independent predictors for PD−L1-positive tumors in univariate analysis. However, only C/T mass retained statistical significance in multivariate analysis. This difference could explain why, during the growth of tumor, the percentage increase in mass is greater than the percentage increase in volume or diameter and mass is more sensitive than volume or diameter.[19] Toyokawa et al[34] identified that adenocarcinomas with PD-L1 expression showed a significantly higher C/T size than those without, which helped confirm our results. From the perspective of pathology, higher C/T mass in adenocarcinomas represents a greater possibility of invasiveness, which coincided with the correlation between PD-L1 expression and poor pathological differentiation

previously identified. To further improve the accuracy of diagnosis, we combined the indicators with 5 statistically significant parameters (absence of surrounding GGO, lobulated sign, pleural indentation, tumor mean CT value, and C/T mass) in the multivariate logistic regression analysis and obtained a larger AUC, indicating that the simultaneous use of multiple indicators can help us better predict PD-L1 expression. The joint diagnostic model further described the possibility of diagnostics and predictions from significant imaging features in multivariate analyses. It might provide support for the discussion of treatment options by radiologists and oncologists.

Our study showed that *EGFR* mutation status was related to larger tumor maximum diameter and smaller C/T size, C/T volume, and C/T mass. However, Yano et al reported the tumor size in an *EGFR* mutation group was frequently smaller than in a wild type group.[23] Most of the literature shows that the probability of *EGFR* mutation would increase significantly when the tumor was large.[23,35] However, as we discussed, the presence of surrounding GGO was significantly associated with *EGFR* mutation and the ratio of the GGO component could help predict *EGFR* mutation status. In our study, we found that C/T size, C/T volume, and C/T mass in the *EGFR* mutation group was lower than in the wild type group, which was consistent with a previous study.[35] Interestingly, our study showed that PD-L1 expression status was not related to tumor maximum diameter, whereas *EGFR* mutation was related to larger tumor maximum diameter than wild type. PD-L1 expression was related to absence of surrounding GGO, whereas *EGFR* mutation was related to the presence of surrounding GGO. Higher C/T mass was significantly associated with PD−L1-positive tumors and with *EGFR* wild type status. PD-L1 expression was frequently accompanied with *EGFR* wild type status. Our study implied that the correlation between TSCT features with *EGFR* mutation were almost reversed especially in GGO or solid component of tumors.

The current study has several limitations that should be mentioned. First, this study was a retrospective study, which might contribute to selection bias. Second, some imaging signs such as the presence of cysts in our sample were observed in only 32 cases (11.6%), and most of the patients in this study were at the early stage of lung adenocarcinoma. Therefore, more studies need to be done with larger sample sizes and in patients with advanced adenocarcinoma. Third, the expression of PD-L1 is on a continuum, whereas the cutoff value commonly used in the Department of Pathology in our hospital is 5%. Therefore, the relationship between different levels of PD-L1 expression and imaging findings in adenocarcinoma needs further investigation. Moreover, the PD-L1 IHC test lacks universal reference standards and requires a large-scale prospective study. The IHC antibody in our study has only been used for research purposes and not been developed along with any of the checkpoint inhibitors available for lung cancer, but this antibody has undergone extensive comparisons with other antibodies available. Fourth, our study only described the possibility of using diagnostics and predictions from significant imaging features in multivariate analysis, but the clinical applicability of the study still needs to be tested in additional patients for validation. Finally, we did not investigate the effect of intratumor heterogeneity on the expression of PD-L1 although this phenomenon indeed existed.[36]

Conclusion

We comprehensively investigated the association of imaging features with PD-L1 expression and *EGFR* mutation in surgically treated lung adenocarcinomas. PD-L1 expression was significantly associated with pathologic invasiveness. Absence of surrounding GGO, lobulated sign, pleural indentation sign, tumor mean CT value, and C/T mass were significant factors of differentiating PD−L1-positive tumors from negative ones. Moreover, PD-L1 expression was inversely related to *EGFR* mutational status. *EGFR* mutation was significantly associated with presence of surrounding GGO, larger tumor maximum diameter, and smaller C/T size, C/T volume, and C/T mass. Our study suggested the possibility of predicting PD-L1 expression status in patients with lung adenocarcinoma.

Clinical Practice Points

- Programmed death-ligand 1 ICIs have proved effective and prospective in clinical practice. However, PD-L1 expression varies in different countries according to the existing literature and the correlation between PD-L1 expression and imaging features in lung adenocarcinoma has not been clarified.
- We hoped to confirm whether there is a correlation between PD-L1 expression and imaging features of TSCT. The results showed that 74 of 350 patients (21.1%) were PD−L1-positive and PD-L1 expression was more observed in men and in former/present smokers. PD-L1 expression was frequently significant with invasive adenocarcinomas and adversely associated with *EGFR* mutation status.
- In multivariate logistic regression analysis, the absence of surrounding GGO (OR, 0.4; 95% CI, 0.2-0.9; $P = .022$), lobular/irregular shape (OR, 5.8; 95% CI, 1.6-21.0; $P = .008$), pleural indentation (OR, 2.8; 95% CI, 1.3-5.7; $P = .007$), tumor mean CT value (OR, 4.9; 95% CI, 1.7-14.4; $P = .004$), and C/T mass (OR, 4.7; 95% CI, 1.7-13.0; $P = .003$) were significantly associated with PD-L1 expression.
- We conducted a joint diagnostic model (including all significant imaging features at multivariate analysis) to improve the diagnostic accuracy.
- These results suggested a correlation between PD-L1 expression and imaging features.
- It might also help predict the expression of PD-L1 using CT in patients before they receive immunotherapy.

Disclosure

The authors have stated that they have no conflicts of interest.

Supplemental Data

Supplemental tables and figure accompanying this article can be found in the online version at https://doi.org/10.1016/j.cllc.2018.10.012.

References

1. Goldstraw P, Chansky K, Crowley J, et al. The IASLC Lung Cancer Staging Project: proposals for revision of the TNM stage groupings in the forthcoming (eighth) edition of the TNM classification for lung cancer. *J Thorac Oncol* 2016; 11:39-51.
2. Oken MM, Hocking WG, Kvale PA, et al. Screening by chest radiograph and lung cancer mortality: the Prostate, Lung, Colorectal, and Ovarian (PLCO) randomized trial. *JAMA* 2011; 306:1865-73.

3. Maemondo M, Inoue A, Kobayashi K, et al. Gefitinib or chemotherapy for non−small-cell lung cancer with mutated EGFR. *N Engl J Med* 2010; 362:2380-8.
4. Su C, Zhou F, Shen J, Zhao J, O'Brien M. Treatment of elderly patients or patients who are performance status 2 (PS2) with advanced non−small-cell lung cancer without epidermal growth factor receptor (EGFR) mutations and anaplastic lymphoma kinase (ALK) translocations−still a daily challenge. *Eur J Cancer* 2017; 83:266-78.
5. Zhou F, Zhou C. Lung cancer in never smokers—the East Asian experience. *Transl Lung Cancer Res* 2018; 7:450-63.
6. Wu YL, Zhou C, Hu CP, et al. Afatinib versus cisplatin plus gemcitabine for first-line treatment of Asian patients with advanced non−small-cell lung cancer harbouring EGFR mutations (LUX-Lung 6): an open-label, randomised phase 3 trial. *Lancet Oncol* 2014; 15:213-22.
7. Shaw AT, Kim DW, Nakagawa K, et al. Crizotinib versus chemotherapy in advanced ALK-positive lung cancer. *N Engl J Med* 2013; 368:2385-94.
8. Shaw AT, Ou SH, Bang YJ, et al. Crizotinib in ROS1-rearranged non−small-cell lung cancer. *N Engl J Med* 2014; 371:1963-71.
9. Camidge DR, Pao W, Sequist LV. Acquired resistance to TKIs in solid tumours: learning from lung cancer. *Nat Rev Clin Oncol* 2014; 11:473.
10. Konishi J, Yamazaki K, Azuma M, Kinoshita I, Dosaka-Akita H, Nishimura M. B7-H1 expression on non−small-cell lung cancer cells and its relationship with tumor-infiltrating lymphocytes and their PD-1 expression. *Clin Cancer Res* 2004; 10:5094-100.
11. Topalian SL, Hodi FS, Brahmer JR, et al. Safety, activity, and immune correlates of anti−PD-1 antibody in cancer. *N Engl J Med* 2012; 366:2443-54.
12. Taube JM, Klein AP, Brahmer JR, et al. Association of PD-1, PD-1 ligands, and other features of the tumor immune microenvironment with response to anti−PD-1 therapy. *Clin Cancer Res* 2014; 20:5064-74.
13. Pan Y, Zheng D, Li Y, et al. Unique distribution of programmed death ligand 1 (PD-L1) expression in East Asian non−small-cell lung cancer. *J Thorac Dis* 2017; 9:2579-86.
14. Shukuya T, Carbone DP. Predictive markers for the efficacy of anti−PD-1/PD-L1 antibodies in lung cancer. *J Thorac Oncol* 2016; 11:976-88.
15. Chen Y, Mu CY, Huang JA. Clinical significance of programmed death-1 ligand-1 expression in patients with non−small-cell lung cancer: a 5-year-follow-up study. *Tumori* 2012; 98:751-5.
16. Dai J, Shi J, Soodeen-Lalloo AK, et al. Air bronchogram: a potential indicator of epidermal growth factor receptor mutation in pulmonary subsolid nodules. *Lung Cancer* 2016; 98:22-8.
17. Rizzo S, Petrella F, Buscarino V, et al. CT radiogenomic characterization of EGFR, K-RAS, and ALK mutations in non−small-cell lung cancer. *Eur Radiol* 2016; 26: 32-42.
18. Liu Y, Sun H, Zhou F, et al. Imaging features of TSCT predict the classification of pulmonary preinvasive lesion, minimally and invasive adenocarcinoma presented as ground glass nodules. *Lung Cancer* 2017; 108:192-7.
19. de Hoop B, Gietema H, van de Vorst S, Murphy K, van Klaveren RJ, Prokop M. Pulmonary ground-glass nodules: increase in mass as an early indicator of growth. *Radiology* 2010; 255:199-206.
20. Rosado de Christenson ML. International Association for the Study of Lung Cancer/American Thoracic Society/European Respiratory Society international multidisciplinary classification of lung adenocarcinoma. *The Yearbook of Diagnostic Radiology* 2012; 2012:2-5.
21. Yang CY, Lin MW, Chang YL, Wu CT, Yang PC. Programmed cell death-ligand 1 expression in surgically resected stage I pulmonary adenocarcinoma and its correlation with driver mutations and clinical outcomes. *Eur J Cancer* 2014; 50: 1361-9.
22. Calles A, Liao X, Sholl LM, et al. Expression of PD-1 and its ligands, PD-L1 and PD-L2, in smokers and never smokers with KRAS-mutant lung cancer. *J Thorac Oncol* 2015; 10:1726-35.
23. Yano M, Sasaki H, Kobayashi Y, et al. Epidermal growth factor receptor gene mutation and computed tomographic findings in peripheral pulmonary adenocarcinoma. *J Thorac Oncol* 2006; 1:413-6.
24. Shimoji M, Shimizu S, Sato K, et al. Clinical and pathologic features of lung cancer expressing programmed cell death ligand 1 (PD-L1). *Lung Cancer* 2016; 98:69-75.
25. Russell PA, Wainer Z, Wright GM, Daniels M, Conron M, Williams RA. Does lung adenocarcinoma subtype predict patient survival? A clinicopathologic study based on the new International Association for the Study of Lung Cancer/American Thoracic Society/European Respiratory Society international multidisciplinary lung adenocarcinoma classification. *J Thorac Oncol* 2011; 6: 1496-504.
26. Azuma K, Ota K, Kawahara A, et al. Association of PD-L1 overexpression with activating EGFR mutations in surgically resected non−small-cell lung cancer. *Ann Oncol* 2014; 25:1935-40.
27. Hashizume T, Yamada K, Okamoto N, et al. Prognostic significance of thin-section CT scan findings in small-sized lung adenocarcinoma. *Chest* 2008; 133:441-7.
28. Haneda H, Sasaki H, Shimizu S, et al. Epidermal growth factor receptor gene mutation defines distinct subsets among small adenocarcinomas of the lung. *Lung Cancer* 2006; 52:47-52.
29. Wang J, Sone S, Feng L, et al. Rapidly growing small peripheral lung cancers detected by screening CT: correlation between radiological appearance and pathological features. *Br J Radiol* 2000; 73:930-7.
30. Morimoto K, Miyahara R, Li M, et al. A pitfall of CT findings in peripheral lung adenocarcinoma. *J Comput Assist Tomogr* 2002; 26:197-8.
31. Toyokawa G, Shimokawa M, Kozuma Y, et al. Invasive features of small-sized lung adenocarcinoma adjoining emphysematous bullae. *Eur J Cardiothorac Surg* 2017; 53:372-8.
32. Woodring J, Fried A, Chuang V. Solitary cavities of the lung: diagnostic implications of cavity wall thickness. *AJR Am J Roentgenol* 1980; 135:1269-71.
33. Lee HY, Choi YL, Lee KS, et al. Pure ground-glass opacity neoplastic lung nodules: histopathology, imaging, and management. *AJR Am J Roentgenol* 2014; 202: W224-33.
34. Toyokawa G, Takada K, Okamoto T, et al. Relevance between programmed death ligand 1 and radiologic invasiveness in pathologic stage I lung adenocarcinoma. *Ann Thorac Surg* 2017; 103:1750-7.
35. Aoki T, Hanamiya M, Uramoto H, Hisaoka M, Yamashita Y, Korogi Y. Adenocarcinomas with predominant ground-glass opacity: correlation of morphology and molecular biomarkers. *Radiology* 2012; 264:590-6.
36. McLaughlin J, Han G, Schalper KA, et al. Quantitative assessment of the heterogeneity of PD-L1 expression in non−small-cell lung cancer. *JAMA Oncol* 2016; 2:46-54.

Supplemental Table 1 *EGFR* Mutation and Clinicopathological Characteristics

	EGFR Mutation-Negative (n = 145)	*EGFR* Mutation-Positive (n = 205)	Total	*P*
Sex				
Male	73 (50.3)	70 (34.1)	143 (40.9)	.002
Female	72 (49.7)	135 (65.9)	207 (59.1)	
Age, y	61.23 ± 9.14	62.73 ± 9.21	62.11 ± 9.20	.080
Smoking History				
Ever smoker	84 (57.9)	63 (30.7)	147 (42.0)	.000
Never smoker	61 (42.1)	142 (69.3)	203 (58.0)	
Location				
LUL	35 (24.1)	38 (18.5)	73 (20.9)	.410
LLL	17 (11.7)	31 (15.1)	48 (13.7)	
RUL	53 (36.6)	65 (31.7)	118 (33.7)	
RML	11 (7.6)	18 (8.8)	29 (8.3)	
RLL	29 (20.0)	53 (25.9)	82 (23.4)	
Pathological Diagnosis				
AAH/AIS/MIA	42 (29.0)	53 (25.9)	95 (27.1)	.519
Invasive subtype	103 (71.0)	152 (74.1)	255 (72.9)	
Pathological Tumor Diameter, cm				
≤2.0	73 (50.3)	93 (45.4)	166 (47.4)	.358
>2.0	72 (49.7)	112 (54.6)	184 (52.6)	
TNM				
a	131 (90.3)	183 (89.3)	314 (89.7)	.744
≥Ib	14 (9.7)	22 (10.7)	36 (10.3)	
PD-L1 Expression				
Negative	95 (65.5)	181 (88.3)	276 (78.9)	.000
Positive	50 (34.5)	24 (11.7)	74 (21.1)	

Data are presented as n (%) or mean ± SD, except where otherwise noted.
Abbreviations: AAH = atypical adenomatous hyperplasia; AIS = adenocarcinoma in situ; LLL = left lower lobe; LUL = left upper lobe; MIA = minimally invasive adenocarcinoma; PD-L1 = programmed death ligand-1; RLL = right lower lobe; RML = right middle lobe; RUL = right upper lobe; TNM = tumor, node, metastases.

Supplemental Table 2 *EGFR* Mutation and Imaging Features

	EGFR Mutation		Univariate Analysis	
	Negative (n = 145)	Positive (n = 205)	OR (95% CI)	*P* Value
Surrounding GGO				
No	58 (40.0)	58 (28.3)	1.7 (1.1-2.7)	.022
Yes	87 (60.0)	147 (71.7)		
Shape				
Round	24 (16.6)	40 (19.5)	0.8 (0.5-1.4)	.481
Lobular/irregular	121 (83.4)	165 (80.5)		
Margin				
Smooth	90 (62.1)	141 (68.8)	0.7 (0.5-1.2)	.192
Speculated/lobulated	55 (37.9)	64 (31.2)		
Cyst				
No	128 (88.3)	183 (89.3)	0.9 (0.5-1.8)	.771
Yes	17 (11.7)	22 (10.7)		
Air Bronchogram				
No	72 (49.7)	93 (45.4)	1.2 (0.8-1.8)	.429
Yes	73 (50.3)	112 (54.6)		
Vessel Convergence Sign				
No	104 (71.7)	134 (65.4)	1.3 (0.8-2.1)	.210
Yes	41 (28.3)	71 (34.6)		
Vascular Invasion				
No	122 (84.1)	176 (85.9)	0.9 (0.5-1.6)	.657
Yes	23 (15.9)	29 (14.1)		
Pleural Indentation				
No	55 (37.9)	72 (35.1)	1.1 (0.7-1.8)	.590
Yes	90 (62.1)	133 (64.9)		
Tumor Maximum Diameter, mm	27.42 ± 13.38	29.54 ± 13.44	2.2 (1.2-4.0)	.008
Tumor				
Size, mm	18.79 ± 8.42	20.06 ± 8.85	2.4 (1.2-4.7)	.011
Mean CT, HU	−267.91 ± 250.20	−305.24 ± 224.04	0.6 (0.4-0.9)	.007
Volume, mm^3	5547.92 ± 6063.25	6634.19 ± 6687.40	2.4 (1.2-4.7)	.011
Mass	4019.69 ± 4024.48	4820.77 ± 5181.80	3.1 (1.4-6.7)	.004
Consolidation				
Size, mm	12.33 ± 9.45	12.12 ± 10.02	0.6 (0.4-1.0)	.044
Mean CT, HU	−179.64 ± 230.55	−185.37 ± 223.92	0.8 (0.5-1.2)	.242
Volume, mm^3	2663.78 ± 3232.49	2945.14 ± 4869.76	0.6 (0.4-1.0)	.047
Mass	2601.02 ± 3222.81	2818.08 ± 4673.88	0.6 (0.4-1.0)	.064
C/T				
Size, mm	0.60 ± 0.42	0.53 ± 0.40	0.6 (0.4-0.9)	.010
Volume, mm^3	0.49 ± 0.45	0.38 ± 0.42	0.6 (0.4-0.9)	.010
Mass	0.51 ± 0.44	0.41 ± 0.42	0.6 (0.4-0.9)	.010

Data are presented as n (%) or mean ± SD, except where otherwise noted.
Abbreviations: CT = computed tomography; C/T = the ratio of consolidation part to the whole tumor; GGO = ground glass opacity; HU = Hounsfield units; OR = odds ratio.

Supplemental Figure 1 Representative Case Image of Programmed Death Ligand-1 (PD-L1) Expression Status. Radiological—Immunohistochemical Correlation in Adenocarcinoma: PD—L1-Positive (A and B) and PD—L1-Negative (C and D)